5-24-2018

Metal-Interface-Elastomer (MINE) Structures for Stretchable Electronics

Tricia Carmichael

Akhil Vohra
University of Windsor

Kory Schlingman
University of Windsor

R. Stephen Carmichael
University of Windsor

Membrane-Interface-Elastomer (MINE) Structures for Stretchable Electronics

*Akhil Vohra, Kory Schlingman, R. Stephen Carmichael, and Tricia Breen Carmichael**

Department of Chemistry & Biochemistry, University of Windsor, Windsor, Ontario, Canada, N9B 3P4

E-mail: tbcarmic@uwindsor.ca

Summary

The future of soft, conformable, and robust wearable electronics will require elastomers to provide mechanical stabilization, a soft surface to interact with human wearers, and a crucial physical barrier to protect stretchable devices from the environment. It is a difficult challenge, however, for a single elastomer to fulfill each of these needs. Here, we present a new approach that fuses a membrane of poly(dimethylsiloxane) (PDMS) onto the surface of a transparent butyl rubber (T-IIR) substrate using an organosilane-based molecular glue. The resulting membrane-interface-elastomer (MINE) structures uniquely combine the surface chemistry of PDMS with the intrinsically low gas permeability of T-IIR for the fabrication of robust stretchable devices. Our most intriguing finding, however, is that the T-IIR-PDMS interface, buried microns below the PDMS surface, exerts a remarkable influence on metal films deposited on the PDMS membrane surface from below, improving stretching and conductance performance by orders of magnitude.

Stretchable electronic devices built on the elastomer PDMS have generated exciting new technologies, such as PDMS-based light-emitting devices that function during stretching for use as wearable displays or biomedical light therapies,[1-4] wearable PDMS-based sensors that monitor human motion,[5] track vital signs,[6] and simulate tactile sensation,[7] and PDMS-based supercapacitors,[8] battery arrays,[9] and solar cells[10] for energy storage. There are many reasons for the dominance of PDMS in stretchable electronics: Along with being soft, stretchable, biocompatible, transparent, and easy to mold, PDMS possesses surface properties that make it easy to integrate with functional electronic materials for stretchable device fabrication.[11] Plasma oxidation increases the wettability of the PDMS surface by generating a hydrophilic silicate layer to enable the deposition of functional materials from solution.[12] Physical vapor deposition (PVD) of metal films on PDMS is an effective way to fabricate stretchable conductors and electrodes that form the backbone of stretchable devices, remaining conductive to 10 – 50% strain depending on careful control over six different experimental parameters.[13,14] This method forms the basis for well-studied methodologies designed to retain conductivity of the metal film to higher elongations, such as configuring the metal films into serpentines[15] or 2D meshes,[16] or using rough surface topographies to alter how metal films crack with stretching, thus distributing strain relief to limit crack propagation and retain conductive pathways through the film.[17,18]

Despite its status as the default elastomer for stretchable electronics, a disadvantage of PDMS is its high permeability to oxygen and water vapor,[19,20] which destroy devices built using oxygen- or moisture-sensitive materials such as organic semiconductors and oxidizable metal films. Left unshielded from materials decomposition, stretchable devices such as organic light-emitting devices[21,22] and organic photovoltaics[23] suffer premature device failure.[20] We previously reported a new alternative to PDMS based on butyl rubber (poly(isobutylene-co-isoprene), IIR),

an elastomer with a low gas permeability used industrially in applications such as the innerliners of automobile tires.[20] This new butyl rubber is smooth, optically transparent, and has a lower oxygen permeation rate (216 ± 3 cc-mm/m^2-day) than that of PDMS (4500 cc-mm/m^2-day). Using transparent butyl rubber (T-IIR) to encapsulate films of organic semiconductors or oxidizable metals like copper and silver prevents detrimental hydrolysis and oxidation reactions; in contrast, the higher oxygen permeation rate of PDMS makes it an ineffective encapsulating material.

Although T-IIR has the advantage over PDMS in the bulk property of gas permeability, it falls short in terms of surface properties. We have previously shown that T-IIR undergoes destructive bond scission reactions in air or oxygen plasma, producing a low density of oxidized functional groups on the surface.[24] Creating a hydrophilic T-IIR surface requires additional chemical treatment with silicon tetrachloride vapor, which deposits a thin, hydrophilic silicate film on the surface, similar to the surface formed by the simple one-step plasma oxidation of PDMS.[12] In the present paper, we further show that PVD of metals – the routine method used to fabricate stretchable conductors on PDMS – produces discontinuous metal films the T-IIR surface that are inoperative as stretchable conductors.

The strengths and weaknesses of T-IIR and PDMS highlight an emerging dilemma in stretchable electronics: It is challenging for a single elastomer to fulfill all the needs of stretchable electronics applications. Here, we present a new concept to solve this conundrum. By fusing a membrane of PDMS over the surface of a T-IIR substrate, we form a layered membrane-interface-elastomer (MINE) structure that combines the advantages of the two elastomers. The PDMS surface renders this new layered composite stable to gold and silver film deposition by PVD; at the same time, the gas barrier properties of the T-IIR substrate protect

silver components from corrosion. We furthermore show that the interface between the PDMS membrane and T-IIR is surprisingly not innocent, and profoundly influences the mechanical and electrical response of metal films on the PDMS membrane surface to stretching.

Results and Discussion

E-beam evaporation produces markedly different metal films on PDMS and T-IIR. 250-Å-thick gold and silver films deposited on the surface of PDMS substrates are conductive, with sheet resistances (R_s) of 1.8 ± 0.2 Ω/sq and 1.3 ± 0.1 Ω/sq, respectively. In contrast, e-beam deposition of gold and silver on the surface of T-IIR substrates results in films that are not electrically conductive. Optical images and SEM micrographs reveal remarkable differences in metal film morphologies on the two elastomers that explain the differences in conductivity. Gold and silver uniformly coat the PDMS surface to produce consistent films with characteristic wrinkles due to compressive strain in the film that arises from thermal expansion of the PDMS substrate during the e-beam evaporation process (Figure 1a, b; S1a).[25] Gold and silver films on T-IIR, however, appear inhomogeneous and are populated with pinhole defects (Figure 1c, S1b). SEM analysis of a gold film on T-IIR shows a discontinuous film morphology, with gold grains separated by voids up to ~40 nm wide (Figure 1d).

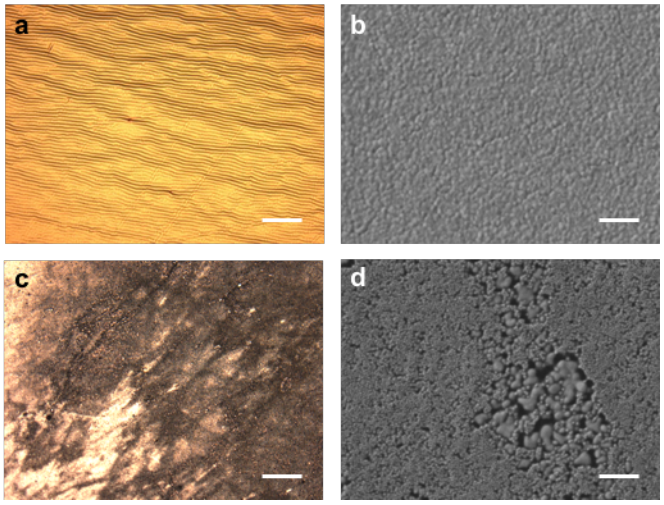

Figure 1. Gold film deposition on PDMS and T-IIR. a, b Optical micrograph (a) and SEM image (b) of a 500-Å-thick gold film on PDMS. (c, d) Optical micrograph (c) and SEM image (d) of a 500-Å-thick gold film on T-IIR. (optical image scale = 200 μm; SEM image scale = 100 nm)

To enable the e-beam deposition of continuous metal films, we fabricated a MINE structure consisting of a thin membrane of PDMS fused to the surface of T-IIR. Simply spin-coating and curing 10:1 PDMS prepolymer on the surface of T-IIR is not a viable method since phosphorus and styrene in the T-IIR formulation are known catalyst poisons that inhibit the platinum-catalyzed curing of PDMS.[26,27] Instead, we adhered a cured PDMS membrane to the T-IIR surface using a two-part organosilane-based "molecular glue", in which a (3-glycidyloxypropyl)trimethoxysilane (GPTMS) monolayer on the T-IIR surface and a (3-aminopropyl)triethoxysilane (APTES) monolayer on the PDMS membrane adhere the two elastomers together through the ring-opening reaction between the terminal amine of APTES and the epoxide of GPTMS (Figure 2a).[28] We prepared a 30-μm-thick PDMS membrane by spin-coating 10:1 PDMS prepolymer onto a silicon wafer treated with a (tridecafluoro-1,1,2,2-tetrahydrooctyl)trichlorosilane (FOTS) release layer, and curing the PDMS. Plasma oxidation

creates a thin SiO_2 layer on the PDMS surface,[12] which binds APTES to produce the amine-terminated surface. We deposited GPTMS on the T-IIR surface using our previously reported method, in which a plasma oxidation step initially produces a low density of oxidized functional groups on the surface.[24] Subsequently exposing this surface to silicon tetrachloride vapor in ambient conditions deposits a thin silicate film on the surface (T-IIR/SiO_2), which then supports the formation of the GPTMS layer. Bringing the APTES-modified PDMS membrane into conformal contact with the GPTMS-modified T-IIR surface enables the interfacial ring opening reaction, adhering the PDMS membrane to the surface of T-IIR to yield the PDMS-T-IIR MINE structure, which we term MINE-30 to denote the PDMS membrane thickness (Figure S2).

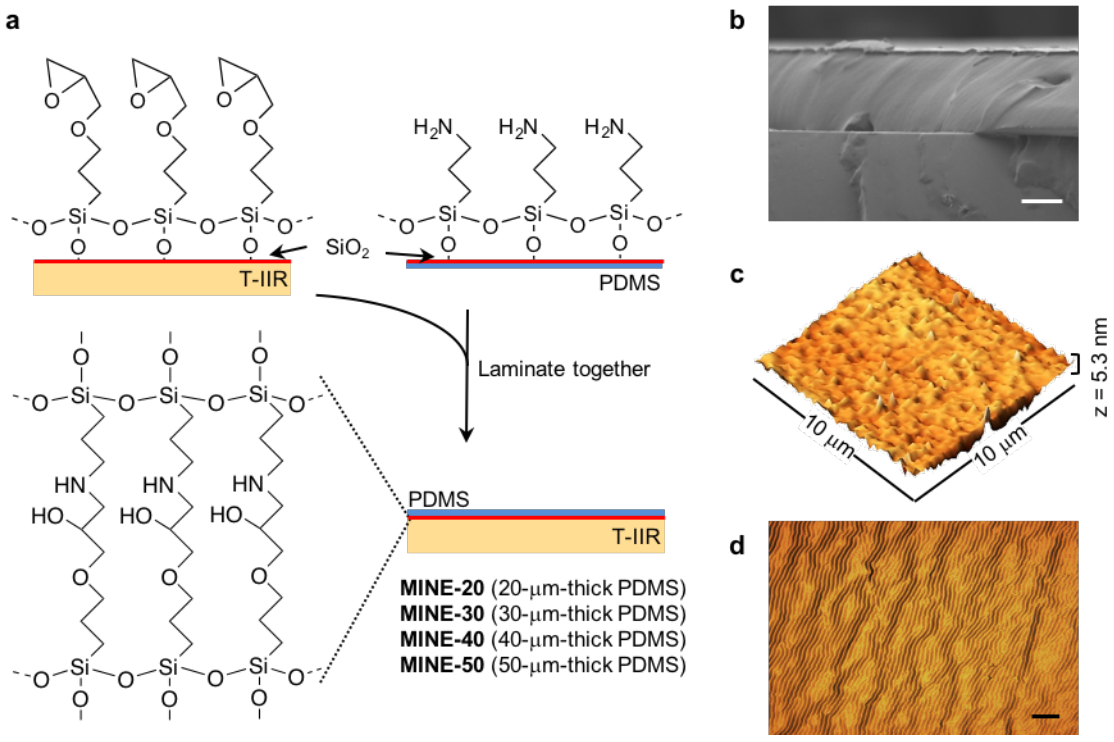

Figure 2. The MINE composite. (a) Fabrication scheme. (b) SEM cross-section of MINE-30 (scale = 15 μm). (c) AFM topographic image of MINE-30. (d) Optical micrograph of a 250-Å-thick gold film deposited on MINE-30 (scale = 200 μm).

MINE-30 is a robust layered composite with a smooth PDMS surface. Cross-sectional scanning electron microscopy (SEM) shows the PDMS membrane with a thickness of ~29 μm adhered to the underlying T-IIR substrate (Figure 2b). Strong adhesion between the two components enables the composite to withstand delamination until 145% elongation (Figure S3). AFM analysis shows the PDMS membrane surface is uniform and smooth (Figure 2c), with a root-mean-square (RMS) roughness (1.8 ± 0.2 nm) typical of native PDMS (1.2 ± 0.3 nm), and lower than that of the rough surface of T-IIR/SiO_2 (40.5 ± 8.7 nm) that comprises the interface. The fabrication of the layered composite has an insignificant effect on the inherent transmittance and clarity of T-IIR, with a transmittance at 550 nm of MINE-30 of 74%, compared to 75% for native T-IIR (Figure S4).

The PDMS membrane of MINE-30 protects the underlying T-IIR substrate from destructive penetration of metal atoms during e-beam deposition, enabling the fabrication of continuous and conductive metal films. Gold and silver films (250 Å in thickness) deposited on MINE-30 (Figure 2d, S5) exhibit wrinkled topographies comparable to those of metal films deposited on PDMS alone using the same deposition parameters (Figure 1a, S1a). The sheet resistances of the metal films on MINE-30 and PDMS alone are all < 2 Ω/sq (Table S1). Despite these initial similarities, the change in resistance that occurs when stretching metal films on the two substrates is strikingly dissimilar. We stretched 2.50 cm x 1.25 cm gold and silver films on PDMS alone and MINE-30 substrates and measured the resistance at 5% strain intervals until the films were no longer conductive. Gold and silver films on PDMS alone remain conductive to 15% elongation, with normalized resistance (R/R_0) values of 323 ± 71 and 1430 ± 237, respectively (Figure 3d, S6d). At 15% strain, gold and silver films on MINE-30 have R/R_0 values of 7 ± 1.3 and 19 ± 1.6, respectively (Figure 3a, S6a). These values are an impressive

~4600% better than gold on PDMS alone, and ~7500% better than silver on PDMS alone. Gold and silver films on MINE-30 also remain conductive to vastly higher elongations (85% and 65%, respectively) than on PDMS alone, with R/R_0 values (93 ± 28 and 560 ± 111, respectively) that remain a fraction of the R/R_0 values on PDMS alone at the inferior strain limit of 15%. Gold films on MINE-30 are also durable to cycles of 15% strain, with R/R_0 remaining ~1 (Figure S7).

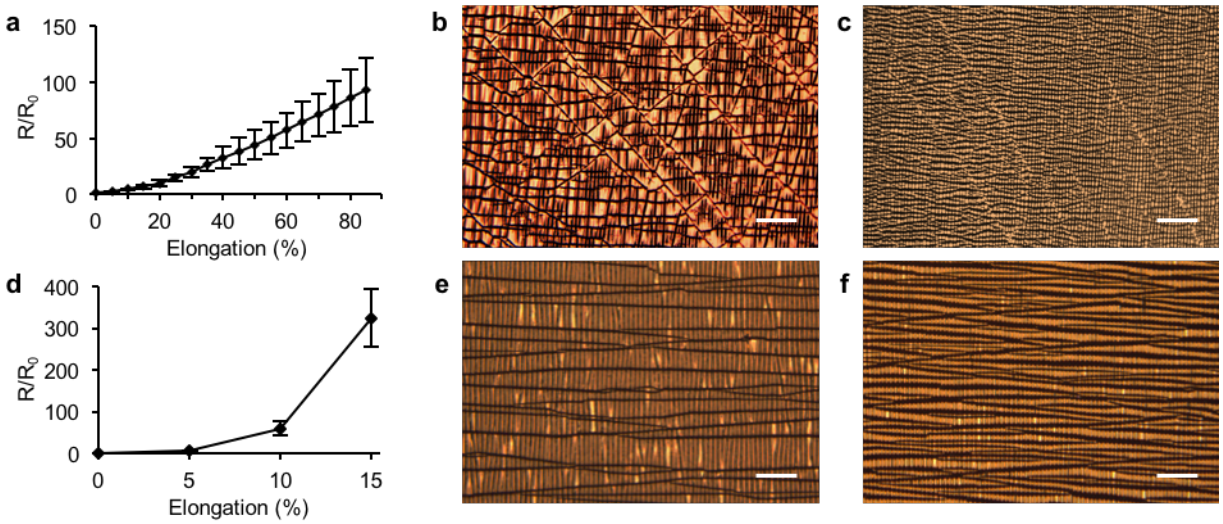

Figure 3. Stretching gold films on MINE-30 and PDMS. (a) Normalized change in resistance of gold films on MINE-30 as a function of elongation. (b, c) Optical micrograph of a gold film on MINE-30 stretched to 15% (b) and 70% (c). (d) Normalized change in resistance of gold films on PDMS as a function of elongation. (e, f) Optical micrograph of a gold film on PDMS stretched to 15% (e) and 70% (f). Samples in b, c, e, f were stretched in the vertical direction, with cracks formed perpendicular to the direction of stretching (scale = 100 μm).

The differences in R/R_0 with stretching between metal films on PDMS alone and on MINE-30 can be attributed to dramatic differences in how cracks in the metal layer evolve with stretching. Stretching stiff metal films adhered to compliant substrates results in the initiation of cracks at defect sites due to strain localization.[29] On PDMS, elongation causes these cracks to

lengthen, which relieves strain but also breaks the conduction pathway at low strains (15%) (Figure 3e, S6e). Further elongation results in the formation of additional channel cracks as well as widening of the cracks from ~4 – 8 μm at 15% strain to ~4 – 12 μm at 70% strain (Figure 3f, S6f). In contrast, stretching metal films on MINE-30 to 15% strain causes the initiation of jagged and disconnected microcracks due to strain localization occurring at numerous sites on the surface (Figure 3b, S6b). These microcracks, which are ~4 – 6 μm in width and vary widely in length, distribute strain relief throughout the film. Unlike metal films on PDMS, additional elongation does not cause these cracks to appreciably widen. Instead, additional cracks develop throughout the metal film to relieve the additional strain (Figure S8), with widths that remain consistently at ~4 – 6 μm (Figure 3c, S6c). SEM images of gold films (Figure 4a, b) on MINE-30 at 40% strain reveal an interlaced pattern of cracks that preserves tortuous pathways necessary for electrical conduction, consistent with the R/R_0 measurements of Figure 3a.

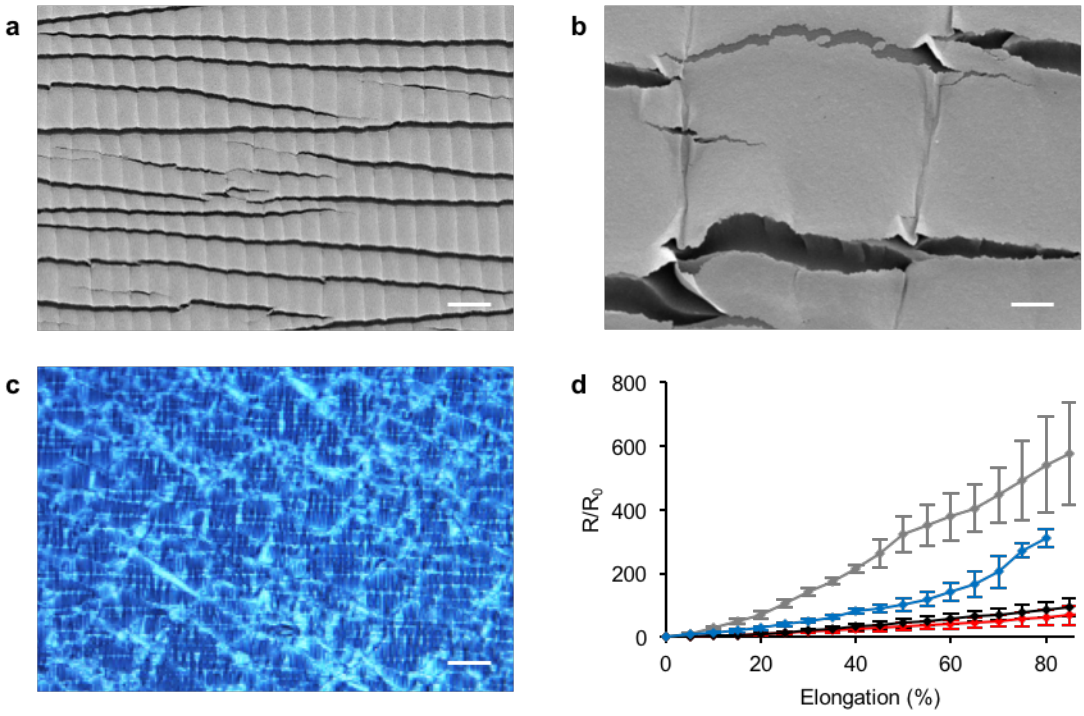

Figure 4. Cracking of gold films on MINE composites. (a, b) SEM images of a gold film at 40% strain on MINE-30 (scale = 20 μm, 2 μm). (c) Optical micrograph of T-IIR/SiO_2 at 40% strain (scale = 60 μm). (d) Normalized change in resistance as a function of elongation for gold films on MINE-20 (red line), MINE-30 (black line), MINE-40 (blue line), and MINE-50 (grey line). In a-c, the samples were stretched in the vertical direction.

What causes the differences in cracking of metal films on bulk PDMS and MINE-30? If we consider only the layers within ~30 μm of the surface, these systems are compositionally identical: Both possess a metal/PDMS interface formed during e-beam evaporation, and optical (Figure 1a, 2d, S1a, S5) and AFM imaging (Figure S9) show that the metal films exhibit similar wrinkles due to compression from the e-beam deposition process. The difference lies deeper below the surface, at the SiO_2 layer between the T-IIR substrate and the PDMS membrane in the MINE-30 structure. SiO_2 is a brittle material that fractures when subjected to stress. Although we

could not image the SiO_2 layer through the top PDMS layer of MINE-30, optical microscopy and AFM of SiO_2 deposited on the T-IIR surface (T-IIR/SiO_2) reveals the fine cracks that form in this layer with stretching (Figure 4c, S10). We postulate that the formation of these cracks perturbs the metal film above, imparting sites for strain localization that subsequently initiate the numerous fine cracks that form in the metal layer with elongation to relieve strain. To test this hypothesis, we prepared MINE structures with thicker PDMS layers (40 μm thickness, MINE-40; 50 μm thickness, MINE-50) to increase the separation between the brittle SiO_2 layer and the gold film. Like gold films on MINE-30, gold films on MINE-40 and MINE-50 show fine cracking patterns (Figure S11). However, as the thickness of the PDMS membrane increases from MINE-30 to MINE-40 to MINE-50, we observe greater increases in resistance as these structures are stretched (Figure 4d). At 80% elongation, R/R_0 for MINE-30 is 86 ± 27, whereas R/R_0 for MINE-40 is 311 ± 31, and R/R_0 for MINE-50 is 541 ± 164. These differences in R/R_0 can be attributed to subtle differences in the cracking of the gold films caused by a diminishing influence of the SiO_2 layer on the gold film as the separation increases. We also tested the effect of bringing the brittle SiO_2 layer closer to the gold coating by fabricating MINE-20, which has a membrane thickness of 20 μm. The thinner membrane of MINE-20 reduces the resistance changes with stretching of gold films compared to the MINE-30 system, consistent with an increased influence of the brittle SiO_2 layer. However, the R/R_0 values at each elongation of MINE-20 are within one standard deviation of the data for MINE-30, suggesting that the SiO_2 layer is exerting its fullest measurable influence over the resistance of the gold film at a 20-30 μm separation. We also conducted a control experiment that omitted the use of silicon tetrachloride vapor to deposit a brittle SiO_2 layer to furthermore establish that this layer is the key factor that influences how metal films crack on the PDMS membrane surface. Since it is not

possible to fabricate MINE-30 composites without using silicon tetrachloride vapor treatment, we instead adhered a 30-μm-thick membrane of PDMS onto a bulk PDMS substrate using the molecular glue protocol. Similar to MINE composites, this PDMS-PDMS layered composite is robust: the PDMS membrane delaminates at 130% elongation (Figure S12b). We deposited a gold film (250 Å in thickness) on the surface and found that both the cracking pattern (Figure S12c) and the conductivity with stretching of these PDMS-PDMS composites is indistinguishable from gold films deposited on bulk PDMS substrates, with an elongation at electrical failure of 15%. Overall, these experiments strongly support the idea that the cracking of the brittle interfacial SiO_2 layer and gold film are connected by stress transfer that occurs over separations of tens of microns.

The PDMS film and SiO_2 interfacial layer of MINE-30 work together to enable the integration of conductive and stretchable metal films with the T-IIR gas-diffusion barrier material. We demonstrate the synergy of all three components of MINE-30 by studying the effect of mechanical and environmental stresses on 250-Å-thick silver films deposited on MINE-30, and on PDMS substrates as a comparison system. We encapsulated these silver films by laminating either a T-IIR film (for MINE-30 substrates) or a PDMS film (for PDMS substrates) over the surface and sealing the edges with a polyurethane adhesive (Clearflex 50) (Figure S13). We exposed the encapsulated silver films to 100% relative humidity (RH) for 24 h in a controlled environment, subjected them to 50 stretch-release cycles of 15% elongation, and then measured the resistance of the films at 0% strain. We repeated this process every 24 h to a total of 480 h humidity exposure and 1000 stretch-release cycles. Optical micrographs (Figure 5a, b) along with plots of the change in resistance as a function of humidity exposure time and the number of strain cycles (Figure 5c), demonstrate how differently the combined environmental

and mechanical stresses affect silver films in MINE-30 and PDMS ensembles. Optical micrographs of MINE-30 ensembles after 480 h of testing show only the expected microcracks due to stretching (Figure 5a). R/R_0 remains < 2 throughout the testing window, showing the tolerance of this system to 1000 cycles of 15% strain and the low permeability of MINE-30 to fully humidified air. R/R_0 for the PDMS ensemble remains comparatively low (< 2) at 144 h of humidity exposure and 300 strain cycles, showing a tolerance to repeated 15% strain. However, R/R_0 increases rapidly thereafter, reaching 5×10^7 by the end of the testing window (480 h), six orders of magnitude greater than MINE-30 ensembles. Optical micrographs of PDMS ensembles after 480 h of testing show the typical cracks due to 15% strain, but also a patina consistent with corrosion (Figure 5b) caused by permeation of humid air through PDMS, resulting in the dramatic increase in R/R_0.[20,30]

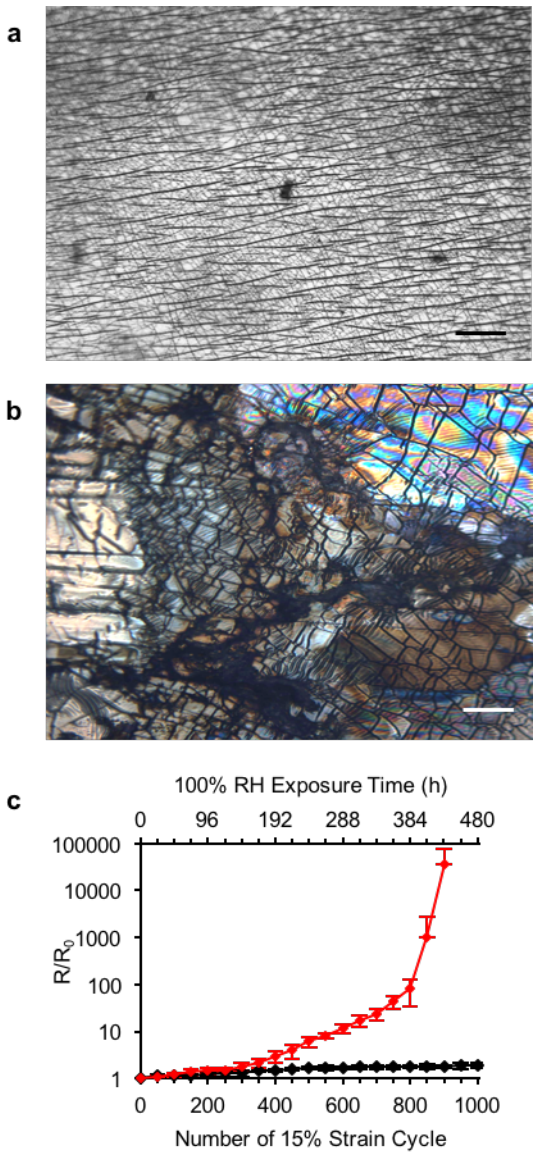

Figure 5. MINE-30 as a gas-diffusion barrier to silver corrosion. (a, b) Optical micrographs of silver films on MINE-30 (a) and on PDMS (b) after 1000 stretch-release cycles of 15% strain and 480 h of exposure to 100% RH (scale = 100 μm). (c) Normalized change in resistance as a function of stretch-release cycles of 15% strain and time of exposure to 100% RH of silver films on MINE-30 (black line) and on PDMS (red line), and encapsulated by T-IIR and PDMS respectively. Samples in a, b were stretched in the vertical direction.

We used stretchable metal films on MINE-30 to demonstrate light-emitting devices that function with stretching and operate in high humidity. We fabricated alternating current electroluminescence (ACEL) devices using thin (250 Å) gold or silver films on MINE-30 as the semi-transparent electrode to permit light emission. The emissive material was ZnS:Cu, which we mixed with PDMS for stretchability and then coated over the electrode surface.[3] We completed the device using a drop of liquid eutectic gallium-indium (EGaIn) as the top electrode (Figure 6a). Figure 6b shows an ACEL device fabricated using a gold electrode in operation at 0% strain and stretched to 50% strain. This device is stable in ambient conditions due to the stability of both the ZnS:Cu emissive material and the gold electrode. Devices fabricated using silver electrodes, however, are susceptible to electrode corrosion and device failure, particularly when operated in high humidity and exacerbated by the high frequency (30 kHz) operation of the device. We fabricated ACEL devices using silver electrodes on both MINE-30 and PDMS substrates, and then encapsulated the devices by laminating T-IIR and PDMS barriers, respectively, over the device surfaces and sealing the edges using waterproof glue (Figure S14). We measured the radiance of the devices initially, and again after 120 h intervals of exposure to 95% RH, to a total of 360 h of humidity exposure. The MINE-30 devices showed a decrease in the radiance of ~10-13% at each 120 h interval (Figure 6c, Table S2); however, this decline is typical of ACEL devices and can be attributed to the structural relaxation at the ZnS-Cu interface resulting in Cu diffusion into the vacancies within the electroluminescent material.[31,32] As a control, we fabricated standard ACEL devices in an oxygen- and moisture-free glovebox using an ITO transparent electrode, ZnS:Cu dispersed in PDMS, and an EGaIn top electrode. These devices exhibited a similar decline in radiance (~10-12%) when characterized after intervals of 120 h in the glovebox (Figure S15), indicating that the decrease in radiance observed form

MINE-30 devices is intrinsic to the ACEL device and not a result of humidity-induced silver electrode corrosion. Support for this idea comes from optical micrographs of the silver electrode of the MINE-30 device after 360 h of humidity exposure, which do not show evidence of corrosion (Figure S16a). In contrast, the radiance of PDMS-based ACEL devices decreased by 99.6% after 360 h of exposure to humidity (from 190.5 ± 42.8 μW to 0.7 ± 0.8 μW) (Figure 6d). Optical micrographs show that this extreme decline in radiance was caused by corrosion of the silver electrodes due to permeation of humid air through the PDMS layers (Figure S16b).

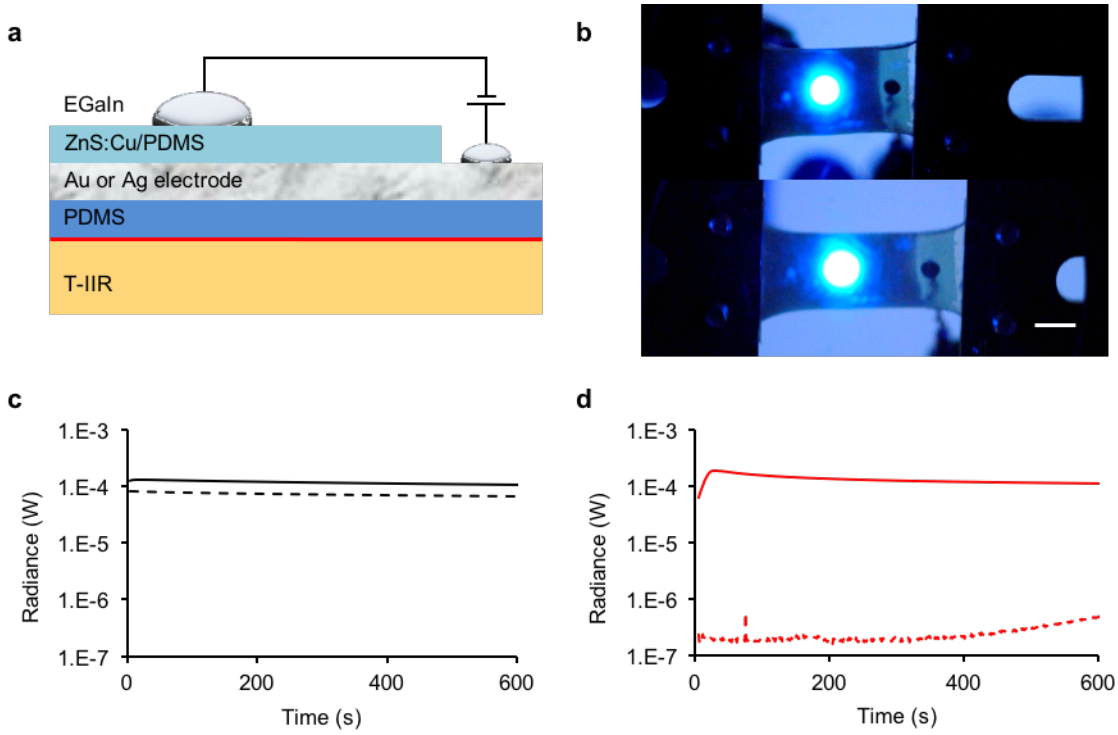

Figure 6. Stretchable and impermeable ACEL devices fabricated on MINE-30. (a) Diagram of ACEL device fabricated on MINE-30. (b) Photograph of an ACEL device fabricated using a gold electrode at 0% (top) and 50% (bottom) strain (scale = 5 mm). (c, d) Radiance response as a function of time before (solid line) and after (dashed line) exposure to 95% RH for 360 h for

ACEL devices fabricated using silver electrodes on a MINE-30 substrate and encapsulated with T-IIR (c), and on a PDMS substrate and encapsulated with PDMS (d).

Conclusion

Combining elastomers into MINE structures is a powerful new design principle that provides unique combinations of properties that a single elastomer cannot deliver. MINE structures of PDMS and T-IIR merge the strengths of these elastomers to produce stretchable conductors that are protected from corrosion by the gas barrier properties of T-IIR. Perhaps most importantly, MINE structures are more than simply the sum of the two elastomeric components. The brittle SiO_2 layer between the elastomers, buried tens of microns below the membrane surface, influences metal films coated above on the membrane surface through stress transfer enabled by the strong interfaces of the MINE composite. This synergy is reminiscent of composite materials such as natural nacre and nacre-mimetic composites, in which stiff inclusions embedded in a soft matrix synergistically cause strengthening and toughening through a mechanism of crack deflection at the inclusion interfaces that effectively dissipates energy.[33] The exciting aspect of MINE structures is that this synergistic effect modifies the electrical function of a partner material coated on the top surface due to the interface that lies microns beneath. This new way to control the properties of coatings provides opportunities for MINE structures to modify the mechanical and electrical behavior of other partner material coatings for a potentially broad range of applications.

Experimental Procedures

PDMS (Sylgard 184) was obtained from Dow Corning, Midland; MI. Clearflex-50 (CF-50) was obtained from Smooth-On, PA. ZnS:Cu microparticles were purchased from Shanghai KPT (EL

Phosphor model D502, 9 μm average particle diameter). T-IIR substrates with a thickness of 0.8 mm were prepared at Lanxess Inc., London, Canada according to previously published methods.[20] All other chemicals were obtained from commercial sources and used as received.

Preparation of APTES-Coated PDMS Membranes Silicon wafers were treated with (tridecafluoro-1,1,2,2-tetrahydrooctyl)trichlorosilane (FOTS) vapor overnight in a vacuum desiccator. PDMS membranes with 30 μm thickness were prepared by spin coating a 10:1 w/w ratio of PDMS prepolymer:curing agent on the FOTS treated silicon wafers at 1000 rpm for 4 min using a Laurell Technologies Model WS-400B spin coater. Changing the spin times varied the thickness of the membrane (10 min for 20 μm, 2 min 30 s for 40 μm thickness, and 2 min for 50 μm thickness).[34] PDMS membranes were cured at 60 °C for 1 h, then treated with air plasma (Harrick Plasma, PDC FMG) generated at the medium RF setting for 40 s at an air pressure of 10 psig (flow rate of 32 mL/min). Oxidized PDMS membranes were immersed in a 1% (v/v) aqueous solution of APTES for 10 min, rinsed with distilled water, and dried in a stream of nitrogen.

Preparation of GPTMS-Coated T-IIR T-IIR substrates (0.8 mm in thickness) were sonicated in acetone and isopropanol for 10 min each, and then treated with oxygen plasma (medium RF) for 15 min at O_2 pressure of 10 psig (flow rate of 10.6 mL/min). The oxidized samples were swabbed with isopropanol, dried in a stream of nitrogen, and suspended for 30 s over a glass Petri dish containing 0.1 mL of silicon tetrachloride in ambient conditions. The samples were then soaked in DI H_2O for 10 min, and dried in a stream of nitrogen. GPTMS was then spin-coated on T-IIR/SiO_2 at 1000 rpm for 1 min, and baked on a hot plate at 100 °C for 10 minutes.

Formation of MINE-30 The GPTMS-coated T-IIR substrate was brought into contact with the APTES-coated PDMS membrane, a glass vial was rolled over the surface to remove air

bubbles, and the composite was left at room temperature for 24 h before peeling away from the silicon wafer.

Metal Deposition MINE-30 and PDMS substrates were oxidized for 40 s in air plasma with an air pressure of 10 psig (flow rate of 32 mL/min), and then e-beam evaporation was used to deposit a 30-Å-thick titanium adhesion layer, followed by either a 250-Å-thick gold film or a 250-Å-thick silver film. A deposition rate of 2.0 Å/s and 1.5 Å/s was maintained for Au and Ag respectively. Ti metal was deposited at a rate of 1.0 Å/s. Six samples were used for all stretchability experiments

Encapsulated Silver Films T-IIR and PDMS films (0.8 mm thick) were laminated on top of silver films deposited on MINE-30 and PDMS substrates (1.25cm x 2.5 cm) respectively, and sealed at the edges using Clearflex-50 (CF-50) adhesive. The ensembles were exposed to 100% RH and 25 °C in a humidity and temperature control chamber. After every 24 h of humidity exposure, the films were subjected to 50 repetitive stretch-strain cycles of 15% strain and the resistance was recorded.

ACEL Device Fabrication ZnS:Cu powder was mixed with PDMS (ZnS:Cu/PDMS) in a weight ratio of 2:1 and spin coated on the metal films on MINE-30 or PDMS at 500 rpm, then cured in an oven for 2 h at 60 °C. A 0.1 mL drop of gallium-indium eutectic (EGaIn) was then deposited on the surface as the top electrode. For encapsulated ACEL devices, T-IIR and PDMS barriers (0.8 mm thick) were laminated on top of the fabricated devices, and the edges of the devices were sealed using butyl (Tremco) or silicone (GE) sealants. Encapsulated ACEL devices were exposed to 95% relative humidity (RH) and 25 °C in a humidity and temperature control chamber. Control ACEL devices were fabricated using ITO as the transparent electrode,

ZnS:Cu/PDMS as emitter, and EGaIn as top electrode. The control devices were fabricated and tested in a glove box.

Characterization A minimum of six samples were included for all reported datasets. Optical characterization was performed using an Olympus BX51 microscope equipped with an Olympus Q-Color3 digital camera. A micro-vice stretcher (S. T. Japan, USA, Inc.) was mounted to the microscope stage and samples were clamped in the stretcher to obtain microscope images of stretched samples. Scanning electron microscopy (SEM) was performed on a Zeiss 1540XB FIB–SEM instrument at the Western Nanofabrication Facility, London, Canada. Scanning electron microscopy of stretched samples was carried out on a Hitachi S-4500 scanning electron microscope at Surface Science Western, London, Canada. Sheet resistance measurements were carried out using a Keithley 2601A Sourcemeter. AFM images were obtained using a Digital Instruments Multimode atomic force microscope run in tapping mode. Veeco type FESP cantilever with a nominal tip radius of 8 nm and a nominal force constant of 2.8 N/m. AFM images were collected over a 10 μm x 10 μm scan area using a scan rate of 0.5 Hz and a scanning resolution of 512 samples/line. Images were collected using Nanoscope 6 software and processed using WSxM 5.0 Develop 8.0 software. Root-mean-square (RMS) roughness values from three different areas of a sample were averaged. For electrical characterization under strain, samples were clamped in a micro-vice stretcher (S.T. Japan, USA, Inc.) and stretched in 5% increments while the resistance was measured with a Keithley 2601A Sourcemeter. EGaIn (~0.05 mL) was deposited by syringe at each end of the wire to facilitate contact to the metal films. A minimum of three samples were tested for each PDMS interlayer thickness. ACEL devices were operated at 5 V DC using Keithley 2601A Sourcemeter connected to a DC-AC

inverter (CXA-series, TDK) with 900 V AC output and frequency of 30 kHz. Radiance was measured with a calibrated UDT S470 optometer attached to an integrating sphere.

Supplemental Information

Supplemental information includes two tables (S1 and S2) and sixteen figures (S1-16) and is available online free of charge.

Author Contributions

T.B.C and R.S.C conceived and designed the experiments; A.V. and K.S. conducted the experiments. All authors analyzed the data and contributed to writing the paper.

Acknowledgements

We dedicate this paper to the memory of our colleague Lorenzo Ferrari. This research was supported by the National Sciences and Engineering Research Council of Canada (NSERC) and LANXESS, Inc. through a Collaborative Research and Development grant (CRDPJ-445264-12). We thank Prof. Simon Rondeau-Gagné for helpful discussions.

References

1. Filiatrault, H.L., Porteous, G.C., Carmichael, R.S., Davidson, G.J.E., and Carmichael, T.B. (2012). Stretchable light-emitting electrochemical cells using an elastomeric emissive material. Adv. Mater. *24*, 2673-2678.
2. Liang, J., Li, L., Niu, X., Yu, Z., and Pei, Q. (2013). Elastomeric polymer light-emitting devices and displays. Nat. Photon. *7*, 817-824.
3. Wang, J., Yan, C., Chee, K.J., and Lee, P.S. (2015). Highly stretchable and self-deformable alternating current electroluminescent devices. Adv. Mater. *27*, 2876-2882.
4. White, M.S., Kaltenbrunner, M., Głowacki, E.D., Gutnichenko, K., Kettlgruber, G., Graz, I., Aazou, S., Ulbricht, C., Egbe, D.A.M., Miron, M.C*., et al.* (2013). Ultrathin, highly flexible and stretchable PLEDs. Nat. Photon. *7*, 811-816.
5. Amjadi, M., Kyung, K.-U., Park, I., and Sitti, M. (2016). Stretchable, skin-mountable, and wearable strain sensors and their potential applications: a review. Adv. Funct. Mater. *26*, 1678-1698.
6. Kim, D.-H., Ghaffari, R., Lu, N., and Rogers, J.A. (2012). Flexible and stretchable electronics for biointegrated devices. Annu. Rev. Biomed. Eng. *14*, 113-128.
7. Lipomi, D.J., Vosgueritchian, M., Tee, B.C.K., Hellstrom, S.L., Lee, J.A., Fox, C.H., and Bao, Z. (2011). Skin-like pressure and strain sensors based on transparent elastic films of carbon nanotubes. Nat. Nanotechnol. *6*, 788-792.
8. Xie, K., and Wei, B. (2014). Materials and structures for stretchable energy storage and conversion devices. Adv. Mater. *26*, 3592-3617.

9. Xu, S., Zhang, Y., Cho, J., Lee, J., Huang, X., Jia, L., Fan, J.A., Su, Y., Su, J., Zhang, H.*, et al.* (2013). Stretchable batteries with self-similar serpentine interconnects and integrated wireless recharging systems. Nat. Commun. *4*, 1543.

10. Lipomi, D.J., Tee, B.C.K., Vosgueritchian, M., and Bao, Z. (2011). Stretchable organic solar cells. Adv. Mater. *23*, 1771-1775.

11. Mark, J.E., Schaefer, D.W., and Lin, G. (2015). The Polysiloxanes (Oxford, Oxford Univ. Press).

12. Chaudhury, M.K., and Whitesides, G.M. (1991). Direct measurement of interfacial interactions between semispherical lenses and flat sheets of poly(dimethylsiloxane) and their chemical derivatives. Langmuir *7*, 1013-1025.

13. Rogers, J.A., Someya, T., and Huang, Y. (2010). Materials and mechanics for stretchable electronics. Science *327*, 1603-1607.

14. Graudejus, O., Görrn, P., and Wagner, S. (2010). Controlling the morphology of gold films on poly(dimethylsiloxane). ACS Appl. Mater. Interfaces *2*, 1927-1933.

15. Jahanshahi, A., Salvo, P., and Vanfleteren, J. (2012). Reliable stretchable gold interconnects in biocompatible elastomers. J. Polym. Sci. Part B Polym. Phys. *50*, 773-776.

16. Shyu, T.C., Damasceno, P.F., Dodd, P.M., Lamoureux, A., Xu, L., Shlian, M., Shtein, M., Glotzer, S.C., and Kotov, N.A. (2015). A kirigami approach to engineering elasticity in nanocomposites through patterned defects. Nat. Mater. *14*, 785-790.

17. Filiatrault, H.L., Carmichael, R.S., Boutette, R.A., and Carmichael, T.B. (2015). A self-assembled, low-cost, microstructured layer for extremely stretchable gold films. ACS Appl. Mater. Interfaces *7*, 20745-20752.

18. Lambricht, N., Pardoen, T., and Yunus, S. (2013). Giant stretchability of thin gold films on rough elastomeric substrates. Acta Mater. *61*, 540-547.

19. Aoki, T. (1999). Macromolecular design of permiselective membranes. Prog. Polym. Sci. *24*, 951-993.

20. Vohra, A., Filiatrault, H.L., Amyotte, S.D., Carmichael, R.S., Suhan, N.D., Siegers, C., Ferrari, L., Davidson, G.J.E., and Carmichael, T.B. (2016). Reinventing butyl rubber for stretchable electronics. Adv. Funct. Mater. *26*, 5222-5229.

21. Scholz, S., Kondakov, D., Lüssem, B., and Leo, K. (2015). Degradation mechanisms and reactions in organic light-emitting devices. Chem. Rev. *115*, 8449-8503.

22. Soltzberg, L.J., Slinker, J.D., Flores-Torres, S., Bernards, D.A., Malliaras, G.G., Abruña, H.D., Kim, J.-S., Friend, R.H., Kaplan, M.D., and Goldberg, V. (2006). Identification of a quenching species in ruthenium tris-bipyridine electroluminescent devices. J. Am. Chem. Soc. *128*, 7761-7764.

23. Hauch, J.A., Schilinsky, P., Choulis, S.A., Rajoelson, S., and Brabec, C.J. (2008). The impact of water vapor transmission rate on the lifetime of flexible polymer solar cells. Appl. Phys. Lett. *93*, 103306-103308.

24. Vohra, A., Carmichael, R.S., and Carmichael, T.B. (2016). Developing the surface chemistry of transparent butyl rubber for impermeable stretchable electronics. Langmuir *32*, 10206-10212.

25. Bowden, N., Brittain, S., Evans, A.G., Hutchinson, J.W., and Whitesides, G.M. (1998). Spontaneous formation of ordered structures in thin films of metals supported on an elastomeric polymer. Nature *393*, 146-149.

26. Bartholomew, C.H. (2001). Mechanisms of catalyst deactivation. Appl. Catal. A *212*, 17-60.

27. Valles, E.M., and Macosko, C.W. (1979). Structure and viscosity of poly(dimethylsiloxanes) with random branches. Macromolecules *12*, 521-526.

28. Lee, N.Y., and Chung, B.H. (2009). Novel poly(dimethylsiloxane) bonding strategy via room temperature "chemical gluing". Langmuir *25*, 3861-3866.

29. Xiang, Y., Li, T., Suo, Z., and Vlassak, J.J. (2005). High ductility of a metal film adherent on a polymer substrate. Appl. Phys. Lett. *87*, 161910-161912.

30. Sharma, S.P. (1978). Atmospheric corrosion of silver, copper, and nickel-environmental test. J. Electrochem. Soc. *125*, 2005-2011.

31. Brese, N.E., Rohrer, C.L., and Rohrer, G.S. (1999). Brightness degradation in electroluminescent ZnS:Cu. Solid State Ion. *123*, 19-24.

32. Popovych, K.O. (2007). Degradation processes in encapsulated ZnS:Cu powder electroluminescent phosphors. Semicond. Phys. Quantum Electron. & Optoelectron. *10*, 77-80.

33. Wang, J., Cheng, Q., and Tang, Z. (2012). Layered nanocomposites inspired by the structure and mechanical properties of nacre. Chem. Soc. Rev. *41*, 1111-1129.

34. Koschwanez, J. H.; Carlson, R. H.; Meldrum, D. R. (2009). Thin PDMS Films Using Long Spin Times or Tert-Butyl Alcohol as a Solvent. PLoS ONE *4*, 1-5.

Table of Contents Graphic

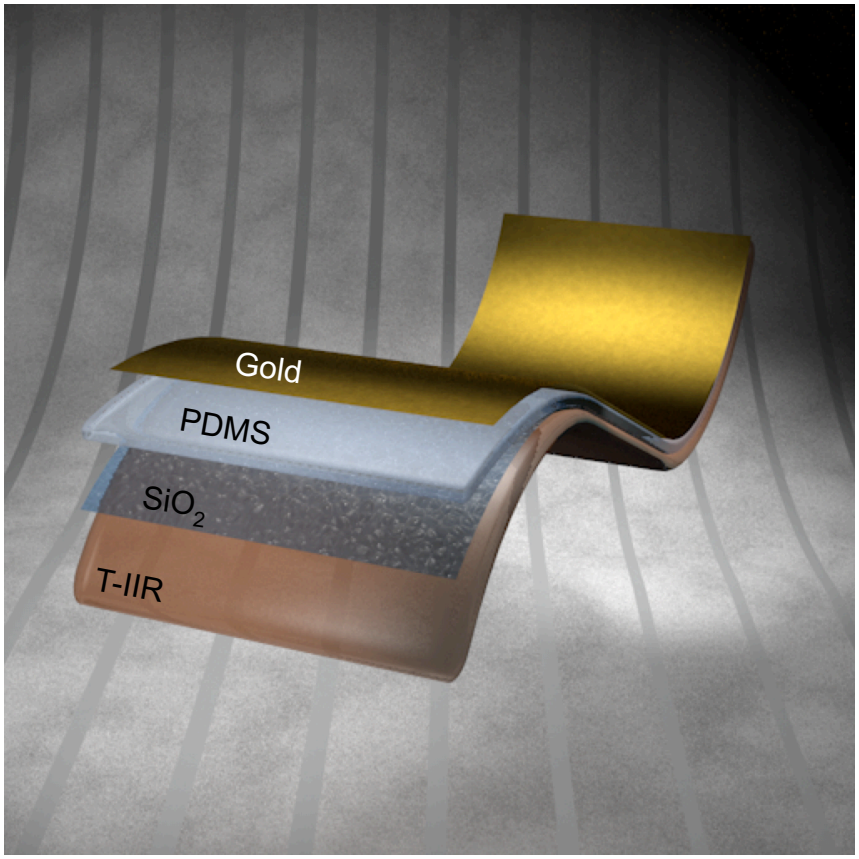

Supporting Information for

Membrane-Interface-Elastomer (MINE) Structures for Stretchable Electronics

*Akhil Vohra, Kory Schlingman, R. Stephen Carmichael, and Tricia Breen Carmichael**

Department of Chemistry & Biochemistry, University of Windsor, Windsor, Ontario, Canada, N9B 3P4

E-mail: tbcarmic@uwindsor.ca

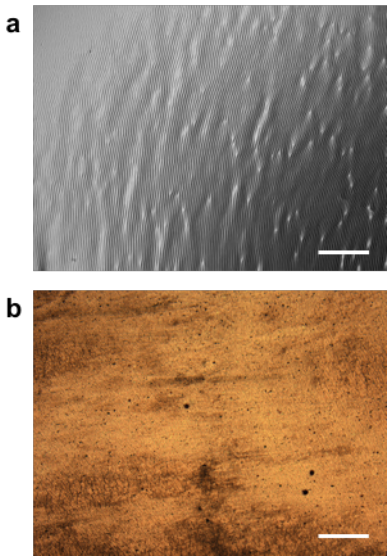

Figure S1 Silver film deposition on PDMS and T-IIR. (a) Optical micrograph of a 250-Å-thick silver film on PDMS. (b) Optical micrograph of a 250-Å-thick silver film on T-IIR. (scale = 400 μm)

Figure S2. Photograph of assembled MINE-30 composite. (scale = 1 cm)

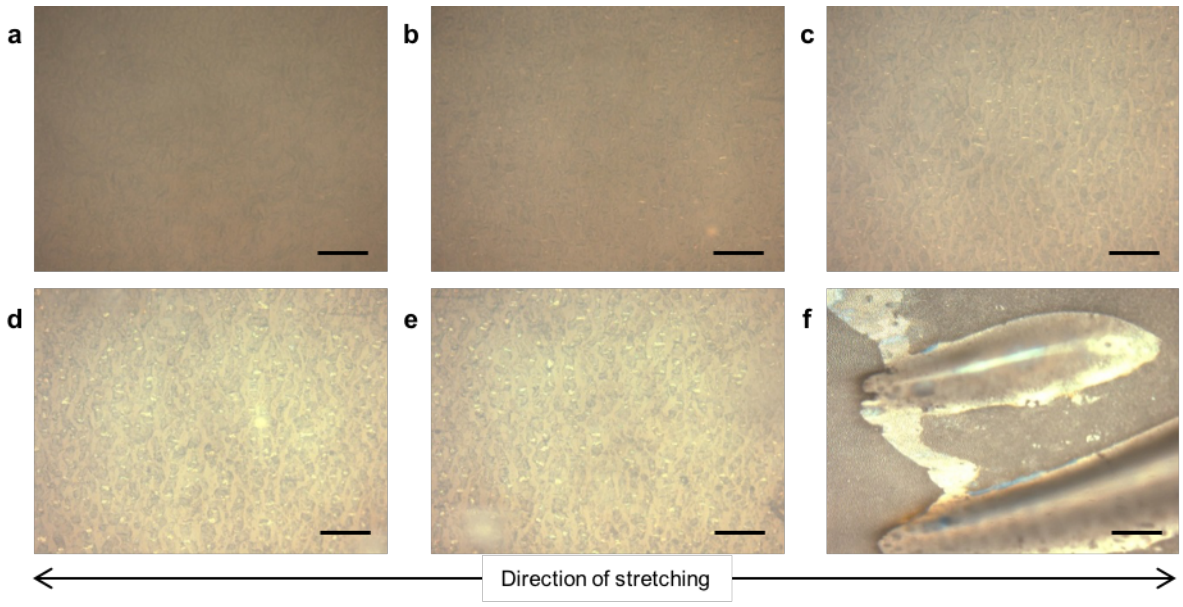

Figure S3. Elongation of MINE-30 layered composites. Optical micrographs at (a) 0%, (b) 25%, (c) 50%, (d) 100%, (e) 125%, (f) 150% strain. (scale = 200 μm)

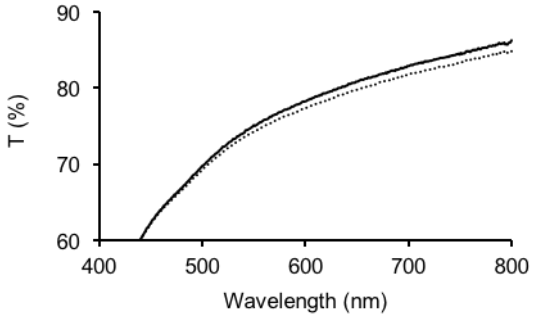

Figure S4. Transmittance spectra of T-IIR (solid line) and MINE-30 (dashed line).

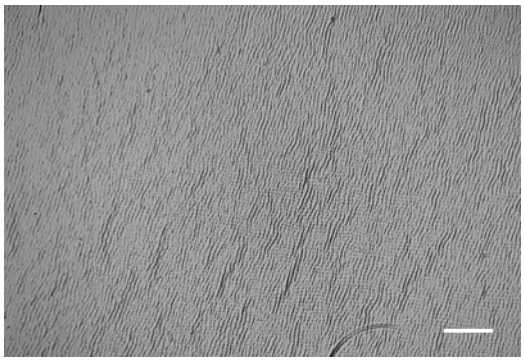

Figure S5. 250-Å-thick silver film on MINE-30 (scale = 100 μm)

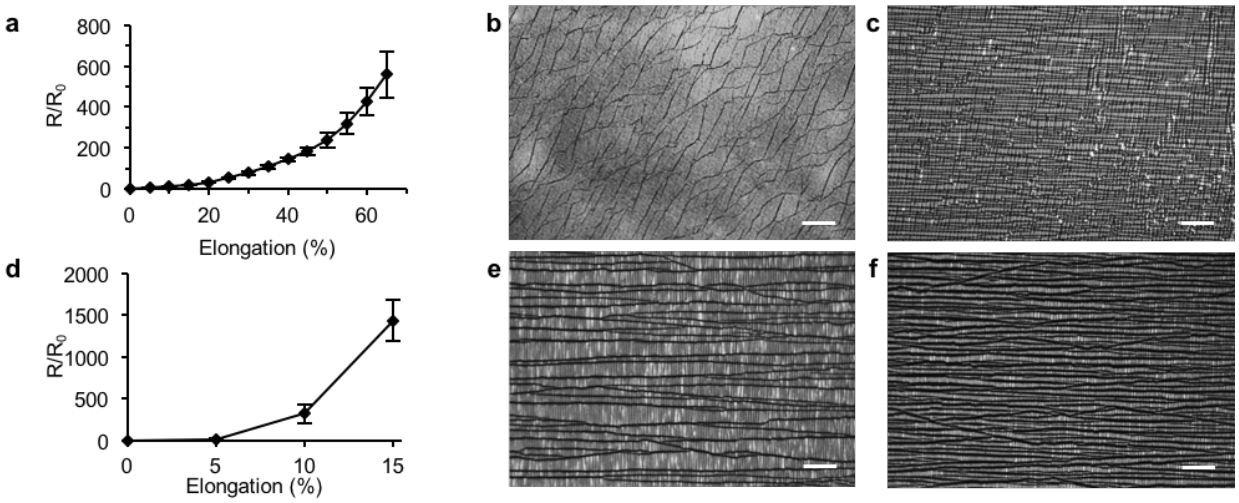

Figure S6. Stretching silver films on MINE-30 and PDMS. (a) Normalized change in resistance of silver films on MINE-30 as a function of elongation. (b, c) Optical micrograph of a silver film on MINE-30 stretched to 15% (b) and 70% (c). (d) Normalized change in resistance of silver films on PDMS as a function of elongation. (e, f) Optical micrograph of a silver film on PDMS stretched to 15% (e) and 70% (f). Samples in b, c, e, f were stretched in the vertical direction (scale = 100 μm).

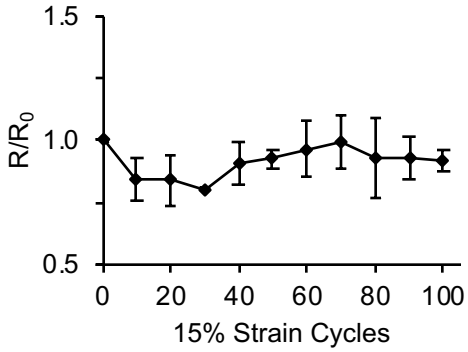

Figure S7. Normalized change in resistance as a function of repetitive stretch-release cycles of 15% strain for 250-Å-thick gold films on MINE-30.

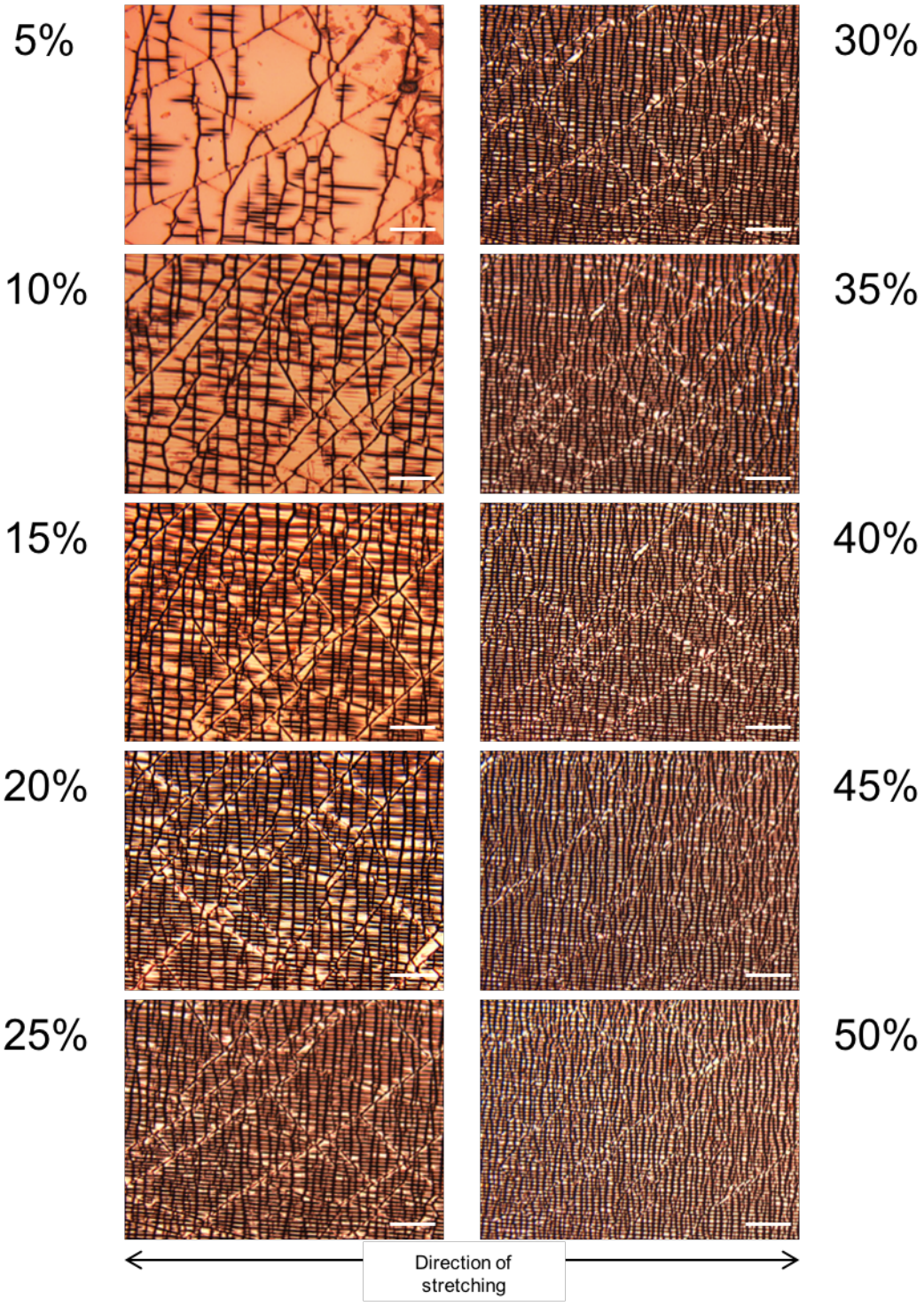

Figure S8. Evolution of cracks with stretching of gold films on MINE-30. Optical micrographs from 5% to 50% strain in 5% increments (scale = 100 μm). Samples were stretched in the horizontal direction.

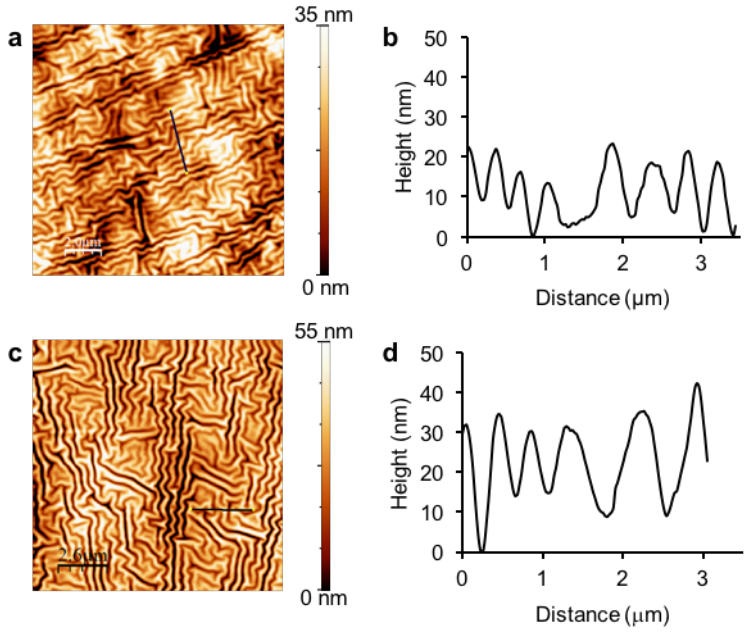

Figure S9. Topography of 250-Å-thick gold films on MINE-30 and PDMS. (a, b) AFM image (a) and height profile (b) of a gold film on MINE-30. (c, d) AFM image (c) and height profile (d) of a gold film on PDMS.

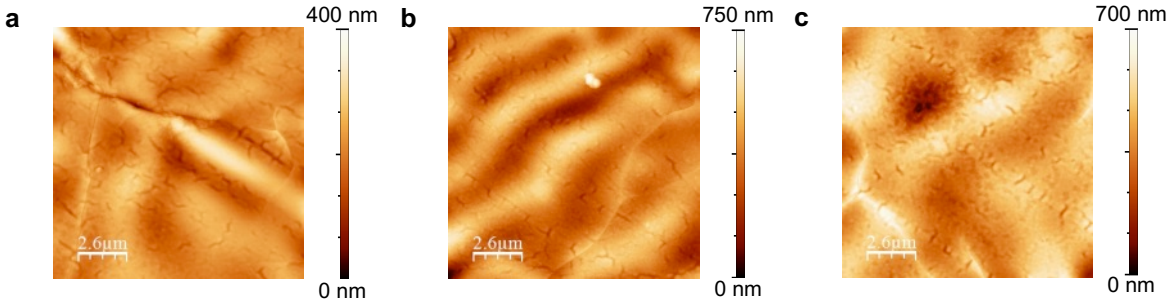

Figure S10. (a-c) AFM topographical images of SiO_2 layer deposited on T-IIR by 30 s of exposure to silicon tetrachloride vapor.

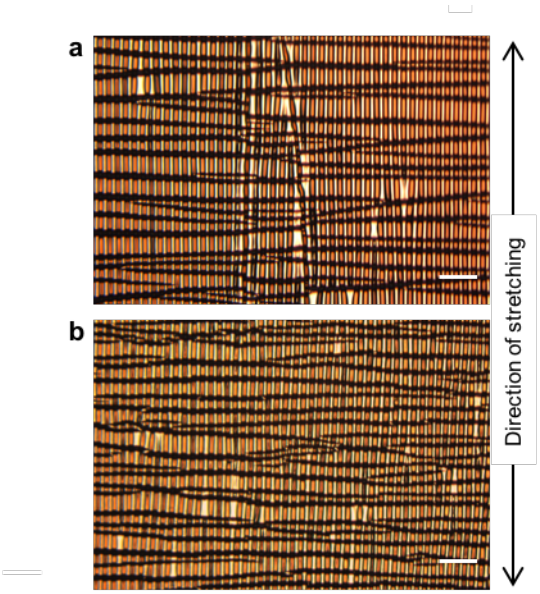

Figure S11. Cracking of gold films on MINE structures. (a, b) Optical images of a gold film on MINE-40 (a) and MINE-50 (b) at 40% strain (scale = 50 μm). Samples were stretched in the vertical direction.

Figure S12. (a) Optical micrograph of 30-μm-thick PDMS film adhered to a bulk PDMS substrate by molecular glue without silicon tetrachloride vapor deposition. (b) Optical micrograph of delamination of the PDMS membrane stretched to 130% elongation. (c) Optical micrograph of a 250-Å-thick gold film deposited on the PDMS membrane surface and stretched to 30% elongation (all scales = 150 μm). Samples were stretched in the horizontal direction.

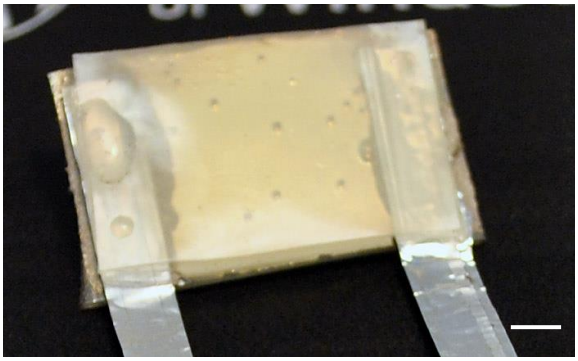

Figure S13. Photograph of silver film encapsulated in MINE-30, sealed with polyurethane adhesive (Clearflex 50). (scale = 0.5 cm)

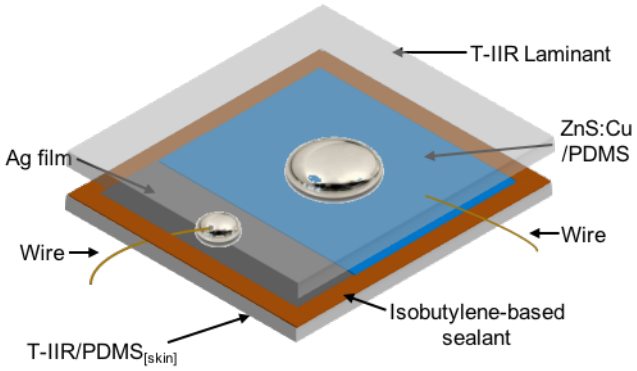

Figure S14. Diagram of sealed ACEL device on MINE-30.

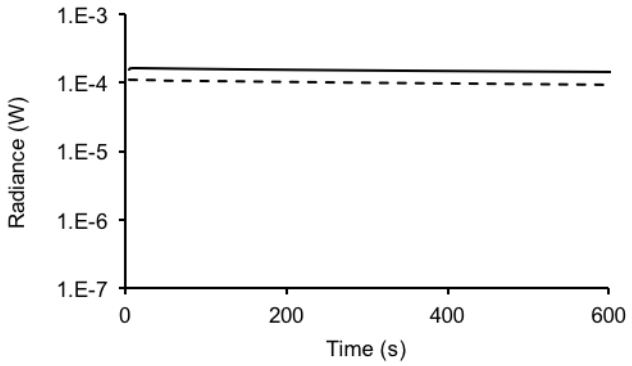

Figure S15. Radiance response as a function of time for an ACEL device fabricated on ITO/glass at 0 h (solid line) and after 360 h (dashed line) in an inert-atmosphere glovebox.

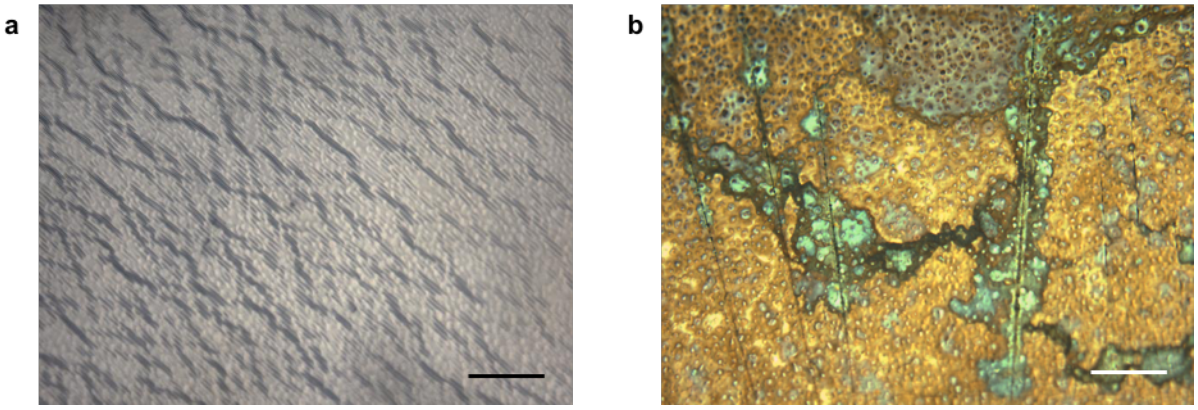

Figure S16. Impermeable ACEL devices fabricated on MINE-30. Optical micrographs of silver electrodes in devices fabricated on a MINE-30 substrate and encapsulated with T-IIR (a), and on a PDMS substrate and encapsulated with PDMS (b) after 360 h exposure to 95% RH. (scale = 100 μm).

Table S1. Sheet Resistances for metal films (250 Å thickness) on MINE-30 and PDMS.

Substrate	Metal	Sheet Resistance (Ω/sq)
MINE-30	Gold	1.8 ± 0.1
MINE-30	Silver	1.2 ± 0.1
PDMS	Gold	1.8 ± 0.2
PDMS	Silver	1.3 ± 0.1

Table S2. Maximum radiance of ACEL devices fabricated on MINE-30 and on PDMS encapsulated by T-IIR and PDMS, respectively, as a function of time in a 95% humidity environment. Maximum radiance of ACEL devices fabricated on ITO are given as a comparison as a function of time in an inert atmosphere.

Time (h)	MINE-30 Max. Rad. (μW)	PDMS Max. Rad. (μW)	ITO Max. Rad. (μW)
0	176.1 ± 17.6	190.5 ± 42.8	151.5 ± 15.8
120	153.3 ± 4.6	94.6 ± 38.8	133.2 ± 11.5
240	135.4 ± 12.6	49.0 ± 80.4	120.3 ± 10.8
360	117.7 ± 13.2	0.7 ± 0.8	108.6 ± 0.4